



Thick Er-doped silica films sintered using CO₂ laser for scintillation applications



Jincheng Lei^{a,b}, Artem A. Trofimov^{b,c}, Jie Chen^d, Zhaoxi Chen^c, Yuzhe Hong^c,
Lei Yuan^{a,b}, Wenge Zhu^{a,b}, Qi Zhang^{a,b}, Luiz G. Jacobsohn^{b,c,**}, Fei Peng^{b,c,*},
Rajendra K. Bordia^c, Hai Xiao^{a,b}

^a Department of Electrical and Computer Engineering, Clemson University, Clemson, SC 29634, USA

^b Center for Optical Materials Science and Engineering Technologies (COMSET), Clemson University, Anderson, SC 29625, USA

^c Department of Materials Science and Engineering, Clemson University, Clemson, SC 29634, USA

^d School of Physics and Electrical Technology, Yancheng Teachers University, Yancheng, Jiangsu 224002, China

ARTICLE INFO

Article history:

Received 30 September 2016

Received in revised form

21 March 2017

Accepted 22 March 2017

Available online 29 March 2017

Keywords:

Scintillation

Silica

Sol-gel

Laser sintering

ABSTRACT

In this work, we demonstrated the fabrication of crack-free luminescent Er-doped silica coatings sintered using a CO₂ laser. The silica sol-gel precursor with controllable rheology was developed using tetraethyl orthosilicate (TEOS) and hexamethyldisiloxane (HMDS). Luminescence activation was achieved through doping with Er ions. Coatings sintered at 1100 °C presented green photoluminescence at ~550 nm and strong radioluminescence as well. After dip-coating, crack-free Er-doped silica thin films were obtained using a CO₂ laser. Films sintered by laser had similar microstructure as the films sintered in a furnace. However, laser sintering extended the thickness range for making crack free sintered films. Using laser sintering, the thickness of crack-free silica films could be extended to above 1 μm, which is important for scintillation and optical waveguide applications. In order to understand the cracking control mechanism, a finite element (FEM) model was developed to analyze the stress distribution within the laser-sintered thin film. The model showed that the localized nature of sintering by laser heating allows for constrained sintering stress relaxation by the softer surrounding region of the film, effectively suppressing cracking.

© 2017 Elsevier B.V. All rights reserved.

1. Introduction

Sol-gel deposition has been a popular methods to fabricate ceramic coatings for scintillation and other optical devices [1–4]. This method requires simple instrumentation compared to other methods like plasma spray and chemical vapor deposition [5,6], and delivers excellent composition controls [7]. Luminescence can be conveniently enabled in coatings prepared by the sol-gel method targeting ionizing radiation and temperature sensing [8,9].

The use of lasers for sintering of sol-gel derived coatings has been investigated since the early 1990s [10]. Unlike traditional furnace sintering, laser sintering can be executed within very short times and with high spatial localization. These advantages

motivated previous studies on sol-gel silica waveguides densified by high power lasers [11–13]. The optical waveguides obtained by laser sintering of coatings on substrates were found to have good dimensional control and optical performance [11–13].

This work is focused on overcoming the critical challenges of laser sintering of sol-gel derived silica coatings concomitant to achieving photoluminescence activation of the coatings targeting the fabrication of miniature silica-based scintillating devices. There are several challenges in executing laser sintering of the sol-gel coatings. First, it is desired to increase the critical thickness of single-layers before cracking occurs during drying and sintering. In most of the previous works on laser densification of sol-gel coatings, the thickness of a single-layer before laser sintering was less than 500 nm [11–13]. While thin layers have lower probability of cracking during laser sintering, single-layers with thickness below ~1 μm cannot be used in common optical devices [14]. Therefore, there is a need to develop processing approaches to make thicker dense coatings.

* Corresponding author. Center for Optical Materials Science and Engineering Technologies (COMSET), Clemson University, Anderson, SC 29625, USA.

** Corresponding author. Center for Optical Materials Science and Engineering Technologies (COMSET), Clemson University, Anderson, SC 29625, USA.

E-mail address: fpeng@clemson.edu (F. Peng).

2. Experimental

2.1. Preparation of Er-doped silica sols and deposition

The silica sols were prepared using tetraethyl orthosilicate (TEOS, $\text{Si}(\text{OC}_2\text{H}_5)_4$, 98%, Sigma-Aldrich, MO, USA) and hexamethyldisiloxane (HMDS, $\text{O}[\text{Si}(\text{CH}_3)_3]_2$, 98.5%, Sigma-Aldrich, MO, USA). HMDS was added to slow down the hydrolysis of TEOS leading to control of the solution rheology [15,16]. For the optimal sol composition, the molar ratio of silicon in HMDS to total silicon was kept at 0.25 to avoid phase separation during condensation. TEOS and HMDS were mixed in ethanol at room temperature inside a glove box under flowing argon. Then deionized water (DI-water) was added into this solution dropwise. A few drops of concentrated nitric acid (HNO_3 , 70%, Sigma-Aldrich, MO, USA) were also added to adjust the pH of the solution to about 2.0. Subsequently, the solution was hydrolyzed at 70 °C for 5 h under vigorous stirring. In order to incorporate Er ions into the sol, erbium nitrate pentahydrate ($\text{Er}(\text{NO}_3)_3 \cdot 5\text{H}_2\text{O}$, Sigma-Aldrich, MO, USA) previously dissolved in ethanol was added into the solution after hydrolysis. The molar ratio of SiO_2 : Er_2O_3 was set at 99.5:0.5. In order to improve the solubility of the Er ions in the silica network to avoid concentration quenching, 1 mol.% of Al_2O_3 to SiO_2 was introduced by means of aluminum nitrate nonahydrate ($\text{Al}(\text{NO}_3)_3 \cdot 9\text{H}_2\text{O}$, Alfa Aesar, MA, USA) into the sol. After stirring at room temperature for 1 h, the sol was refluxed at 70 °C for another 5 h under vigorous stirring. The final solution was kept in an oven at 80 °C until a viscous sol was formed. Part of the viscous sol was kept in the oven until total gelation occurred for thermal analyses. The solid gel was ground and then sintered at 1100 °C for 1 h, and the powder used for photoluminescence measurements.

In order to adjust the viscosity of the sols for dip-coating and to relax stress during firing, poloxamer 407 (Pluronic F127, Spectrum Chemical Mfg. Corp, CA, USA) solution was added into the condensed sol. Poloxamer 407 was dissolved in ethanol with a weight ratio of poloxamer 407:ethanol = 1:9, and then mixed with the sol by high intensity ultrasonic sonication such that the amount of added poloxamer 407 was 50 wt.% of the SiO_2 weight in the sol until a homogeneous and transparent precursor was obtained.

Fused silica substrates were coated with the sols using the dip-coating method. Silica substrates were selected because silica has high absorption in the far infrared wavelength regime and is suitable for CO_2 laser sintering. The thickness of the coatings was controlled by tuning the substrate withdrawing velocity between 60 and 200 mm/min. After deposition, the coatings were dried at room temperature for 1 min.

2.2. Laser sintering of the sol-gel deposition

Fig. 1 shows the schematic of the laser sintering system. A CO_2 laser (firestar v20, SYNRAD, Inc., WA, USA) with a free space wavelength of 10.6 μm was used to process the sol-gel coatings, and a two-axial galvo scanner (intelliSCAN 14, SCANLAB, Germany) was used to control the scanning of the laser beam. A lens with a focal

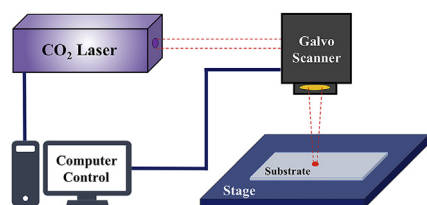


Fig. 1. Schematic of the laser sintering system.

length of 200 mm was used to focus the CO_2 laser beam into a spot with a diameter of ~ 1 mm ($1/e^2$ diameter) on the coatings. Pre-programmed scanning sequences with different scanning velocities and laser powers were used to sinter the coatings. For reference, coatings were fired in a furnace at 1100 °C for 1 h.

2.3. Characterization and simulation

The morphology of the sintered films was characterized by optical microscopy (Olympus BX60, Olympus Corp.) and scanning electron microscopy (SEM, Hitachi S-4800, Hitachi Ltd.). The thickness of the sintered films was measured by atomic force microscopy (AFM, Alpha300, Witec Instruments Corp.). In order to investigate cracking of the laser sintered coatings, the finite element (FEM) modeling software COMSOL Multiphysics was used to simulate the thermal stress distribution of the laser-sintered region.

Photoluminescence spectra were obtained using a spectrofluorometer equipped with double monochromators for both excitation and detection, and a 450 W xenon lamp as the excitation source (Horiba Jobin Yvon Fluorolog 3). All measurements were carried out in ambient conditions with excitation set at 379 nm or monitored at 550 nm, and detection spectral resolution of 1 nm.

Scintillation was evaluated by means of radioluminescence measurements under X-ray excitation using a custom-designed Leksyg Research spectrofluorometer (Freiberg Instruments, Germany) equipped with a VF-50J X-ray tube (Varian Medical Systems, UT) with a W target and operated at 40 kV and 1 mA, and a DU920P-BU Newton CCD camera (Andor Technology, UK). Spectra were not corrected for the spectral response of the system.

3. Results and discussion

3.1. Optimization of the Er-doped silica sols

In order to ensure efficient luminescence of the fired coating as well as to improve the coating ability of the sols, homogeneous sols that are gelable and present controllable rheology are required. Since the gelation process of the TEOS is usually very fast, HMDS was introduced to the sol precursors to slow down the gelation process for better control of the viscosity of the silica sol and to enhance Er dispersion. The compositions of the sol and the gelation behaviors are summarized in Table 1. As shown in Fig. 2A, homogeneous gel can be obtained with precise control of the hydrolysis and polycondensation processes, when the molar percentage of silicon in HMDS is 25% of the total amount of silicon in the solution. This way, the gelation time of the sols could be enhanced to about 24 h, which was nearly 8 times longer than the time without HMDS. After gelation, the gel showed green emission visible to the naked eye when excited by a 378 nm LED (Fig. 3), indicating that the silica sol-gel had been activated by Er ions and that the host was homogeneous at the atomic level. However, when the content of HMDS was increased, precipitation occurred during condensation, thus eliminating the luminescence of Er^{3+} ions due to inhomogeneity of the host material (Fig. 2B and C).

3.2. Luminescence of Er-doped silica

The use of dip-coating method to produce miniature scintillating devices based on silica films requires luminescence functionality. In this proof-of-concept work, luminescence was evaluated by means of photoluminescence, and scintillation by means of radioluminescence measurements. These measurements revealed emission lines corresponding to Er^{3+} $4f-4f$ transitions, and intrinsic emission from the host as shown in Fig. 4. The

Table 1
Composition of the TEOS-HMDS in the sol precursor and the gelation behaviors.

TEOS (mol)	HMDS (mol)	Si _(HMDS) :Si _(total)	Gelation controllability	Gelation time
0.1	0	0	Controllable gelation	~3 h
0.075	0.0125	0.25	Controllable gelation	~24 h
0.05	0.025	0.5	Precipitation	–
0.04	0.03	0.6	Precipitation	–

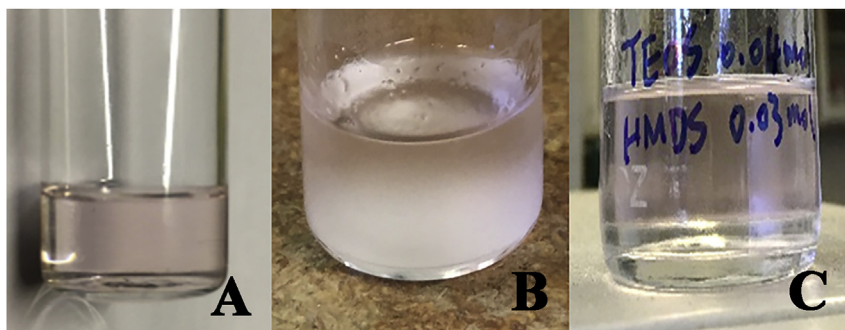


Fig. 2. Photographs of the Er-doped silica sols with different molar percentage of HMDS after thermal treatment in an oven at 80 °C: (A) 25%, (B) 50%, and (C) 60%.

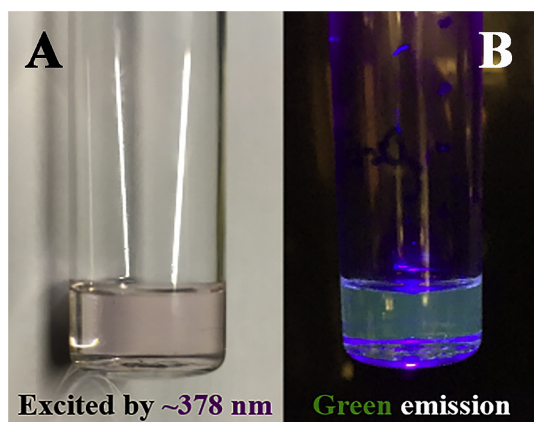


Fig. 3. Photographs of an Er-doped silica gel (A) before and (B) after excitation by a ~378 nm LED.

photoluminescence spectrum of powder fired at 1100 °C for 1 h is shown in Fig. 4A where a series of emission lines at 409, 524, and 548 nm were observed and assigned to the ${}^2\text{H}_{9/2} \rightarrow {}^4\text{I}_{15/2}$, ${}^2\text{H}_{11/2} \rightarrow {}^4\text{I}_{15/2}$, and ${}^4\text{S}_{3/2} \rightarrow {}^4\text{I}_{15/2}$ transitions, respectively [17,18], together with a broad band within ~400–500 nm. The photoluminescence excitation spectrum monitored at 550 nm (Fig. 4B) shows a number of relatively narrow lines that matched the energy levels of the Er^{3+} ion, thus confirming the nature of the luminescence center responsible for the observed emission spectrum obtained under excitation at 379 nm. Photoluminescence measurements of the undoped sample were also executed under 379 nm excitation to check for the contribution of the host to the luminescence signal. These results are shown in Fig. 4C where the presence of two broad bands centered at ~440 nm (2.82 eV) and ~550 nm (2.25 eV) were observed. These bands have been identified to be either from self-trapped excitons or defects like oxygen vacancy and the E' center [19]. Fig. 4D shows that the radioluminescence spectrum of the $\text{SiO}_2:\text{Er}$ sample was dominated by the ${}^2\text{H}_{9/2} \rightarrow {}^4\text{I}_{15/2}$, ${}^2\text{P}_{3/2} \rightarrow {}^4\text{I}_{11/2}$, ${}^2\text{H}_{11/2} \rightarrow {}^4\text{I}_{15/2}$, and ${}^4\text{S}_{3/2} \rightarrow {}^4\text{I}_{15/2}$ transitions, as indicated in the figure, together with a broad contribution between ~300 and 500 nm. Fig. 4E shows the

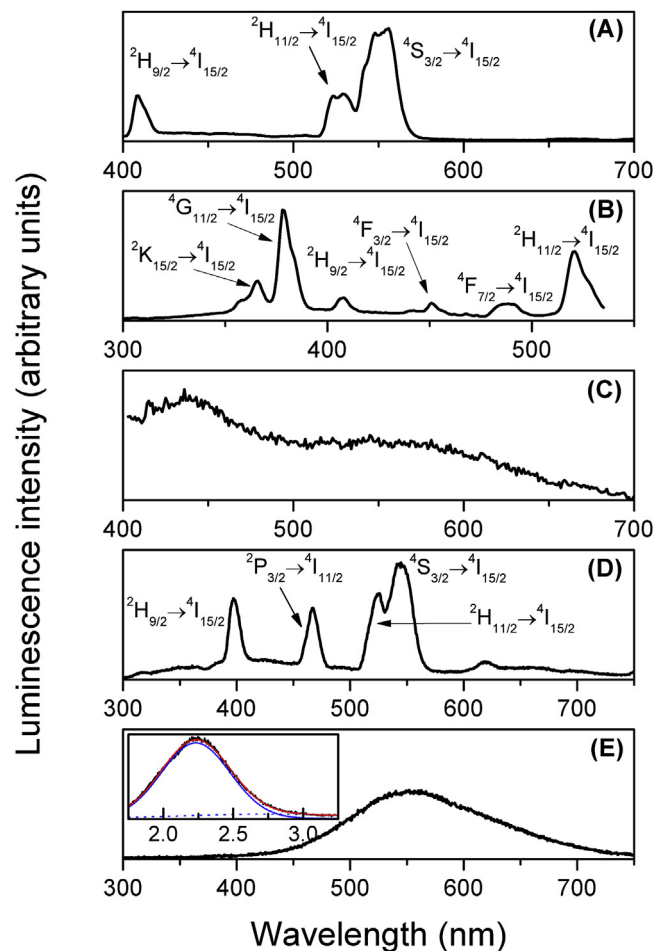


Fig. 4. (A) Photoluminescence spectrum of $\text{SiO}_2:\text{Er}$ under 379 nm excitation; (B) Photoluminescence excitation of $\text{SiO}_2:\text{Er}$ monitored at 550 nm; (C) Photoluminescence spectrum of SiO_2 under 379 nm excitation; (D) Radioluminescence spectrum of $\text{SiO}_2:\text{Er}$; and (E) Radioluminescence spectrum of SiO_2 . The inset shows the results of Gaussian deconvolution as a function of the photon energy in eV (blue lines for the individual components; red line for the fitting). (For interpretation of the references to colour in this figure legend, the reader is referred to the web version of this article.)

radioluminescence spectrum of the undoped sample that is composed by a broad band. The results of Gaussian deconvolution of this band (black line) are shown in the inset as a function of the photon energy and revealed the presence of two bands (blue lines) centered at 450 nm (2.75 eV) and 555 nm (2.23 eV), in good agreement with photoluminescence results shown in Fig. 4C and with the literature. Emission within about 400–550 nm was reported from SiO₂ prepared by sol-gel [18], and within about 350–450 nm from oxygen vacancies in thermally oxidized SiO₂ layers [20]. It is noted that the emission line at 467 nm was assigned to the transition $^2P_{3/2} \rightarrow ^4I_{11/2}$, in agreement with a cathodoluminescence investigation of YAG:Er [21]. The reason for this emission line to appear only in the radioluminescence spectrum is explained by the fact that the $^2P_{3/2}$ energy level is inaccessible to the excitation used in the photoluminescence measurements (379 nm). In summary, the strongest emission lines obtained under X-ray excitation match the range of maximum detection efficiency of photomultiplier tubes commonly used in scintillation applications. These results confirmed that silica could be activated by rare earths to produce efficient luminescence.

3.3. Characterization of the laser-sintered Er-doped silica thin films

Coatings with thickness of $\sim 0.9 \mu\text{m}$ and $\sim 3 \mu\text{m}$ were obtained with substrate withdrawing velocities of 80 and 200 mm/min, respectively. Scratches were intentionally made perpendicular to the scanning path on the deposited films using a blade before laser scanning, as shown in Fig. 5A. Fig. 5 shows optical images of the sample sintered under 7 W laser irradiation at a scanning speed of 1 mm/s. After scanning, a 10 mm track with a width of $\sim 750 \mu\text{m}$ was observed. The scratches were still visible after laser sintering, which means that the film was not significantly ablated by the laser beam. SEM micrographs did not reveal the presence of cracks in the coatings after laser sintering for both the films.

In order to further confirm that the film was not removed by the laser beam as well as to measure its thickness, AFM measurements were carried out to image the edge of the scratch to obtain the height difference between the coating and the substrate. These results are shown in Fig. 6. It is clear that the films stayed on the substrate for both cases. These results also revealed that the films shrank, consistent with sintering during laser scanning. Based on the thickness values before and after laser sintering, the shrinkage

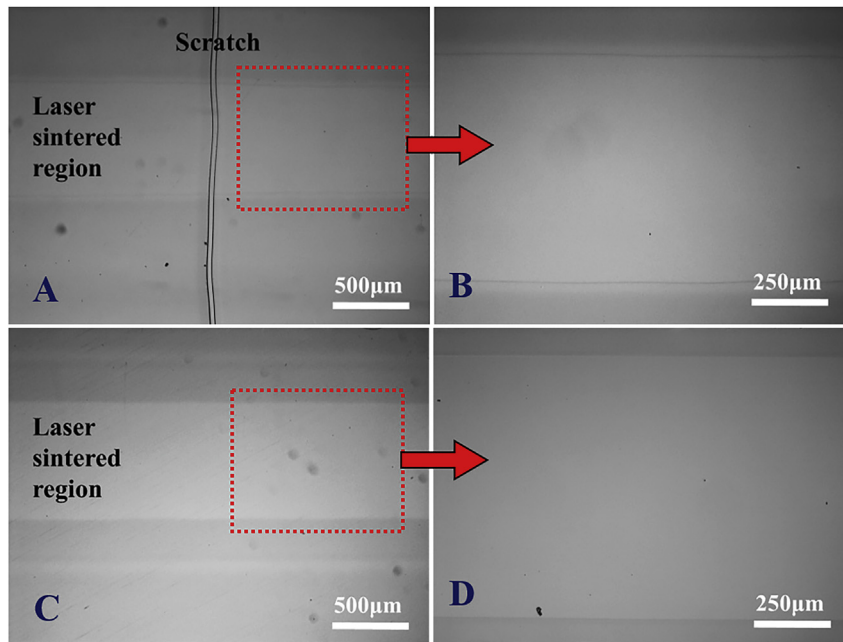


Fig. 5. Optical images (A and C) and SEM micrographs (B and D) of the surface of the laser sintered Er-doped silica thin film (laser output power: 7 W, scanning speed 1 mm/s). (A) Sample with original thickness of $\sim 0.9 \mu\text{m}$, (C) sample with original thickness of $\sim 3 \mu\text{m}$, (B) and (D) are high magnification images of (A) and (C), respectively.

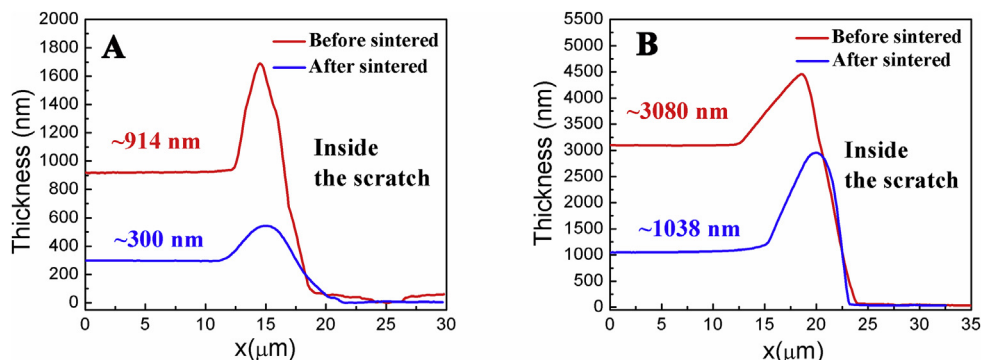


Fig. 6. Thickness of the thin films measured by AFM after 7W laser scanning with speed of 1 mm/s. (A) Original thickness of $\sim 914 \text{ nm}$, and (B) original thickness of $\sim 3080 \text{ nm}$.

Table 2
Shrinkage ratio of the thin films sintered at different conditions.

Condition	Before sintering (nm)	After sintering (nm)	Shrinkage ratio
Laser, 7 W, 1 mm/s	914	300	67.2%
Laser, 7 W, 1 mm/s	3080	1038	66.3%
Furnace, 1100 °C, 1 h	920	293	68.2%

ratio of the coating was calculated (Table 2). Comparison of the shrinkage ratio of the laser sintered coating with the furnace sintered showed all these samples exhibited a similar shrinkage ratio of ~67%.

The evolution of the morphology of the coatings before and after laser sintering, as well as the furnace sintered, was evaluated by SEM. (Fig. 7). As shown in Fig. 7B, there were many voids between the particles before sintering, and after laser sintering the film became denser (Fig. 7D). The interface between the substrate and the coating was hardly discernable. When compared with the high magnification image of the furnace sintered film and the silica substrate all of them showed similar morphologies. This indicated that $>1 \mu\text{m}$ silica coatings can be densified to a similar level as it can be obtained by means of traditional furnace sintering.

3.4. Cracking control of the laser sintering technology

Fig. 8 present optical microscopy images of films thermally treated by laser beam and using a conventional furnace. Fig. 8A

shows that in the central region that was thermally treated by the laser beam, no cracking occurred, while Fig. 8B shows that significant cracking and delamination occurred in the film treated in a furnace at 1100 °C for 1 h. After imaging, the laser sintered film was heat-treated in a furnace at 1100 °C for 1 h. It was found that the area not sintered by the laser beam cracked with the spacing of the cracks being about 700 μm while the laser scanned region remained crack-free and smooth. These results show that for relatively thick sol-gel derived films ($\sim 1 \mu\text{m}$), cracking and delamination can be prevented by laser sintering.

In order to understand the cracking control mechanism of laser sintering, a FEM model was developed to evaluate the stress distribution on the sol-gel derived film during laser sintering.

The simulation concept is similar to the 'strained substrate model' developed by Crosskreutz and McNeil [22], and further expanded by Evans and his coworkers [23]. Due to symmetry considerations, it is possible to consider stress to be one-dimensional. The simulation schematic is shown in Fig. 9 and the relevant parameters are listed in Table 3. In the model, the thin film

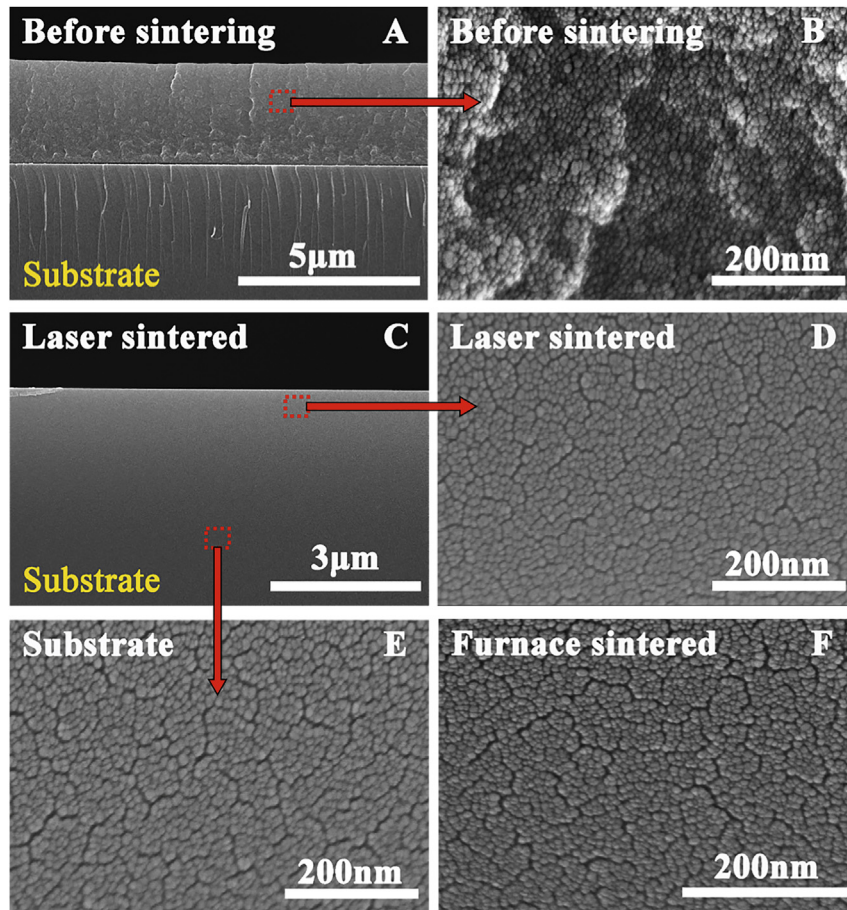


Fig. 7. SEM images of the cross section of a silica coating show that the laser sintered silica film had same microstructure as the furnace sintered sample. (A) Before sintering, low magnification, (B) high magnification image of the coating before sintering, (C) After sintering, low magnification, (D) high magnification image of the coating after laser sintering, (E) high magnification image of the substrate, (F) high magnification image of the furnace sintered coating.

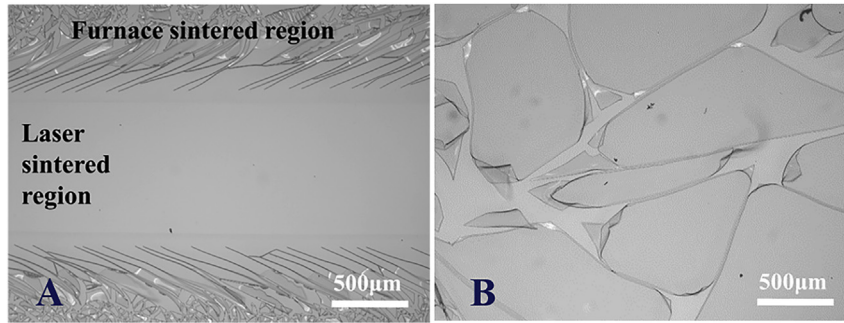


Fig. 8. (A) Optical microscopy images of the laser sintered film after thermal treatment in furnace at 1100 °C for 1 h, and (B) film thermally treated in furnace at 1100 °C for 1 h.

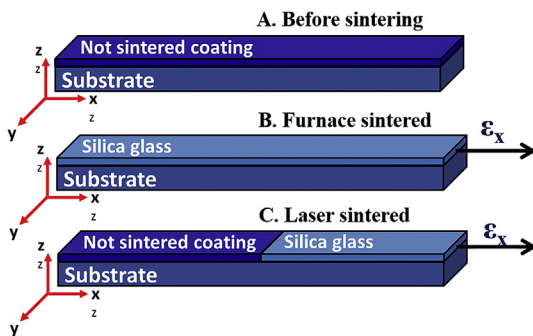


Fig. 9. Simulation schematic of the stress distribution models: (A) before sintering, (B) furnace sintered, and (C) laser sintered.

Table 3
Parameters of simulation.

Parameter	Symbol	Unit	Value
Young's Modulus of silica	E_s	GPa	73.1
Young's Modulus of soft gels	E_g	GPa	2
Applied strain	ϵ_x	—	0.013%

was coated on the silica glass substrate. Since a polymer additive was added into the sols before dip-coating, after deposition on the substrate and drying, the coating was much softer than the substrate. Consequently, the Young's modulus of the coating before sintering was assumed to be close to the polymer additive estimated to be 2 GPa. When treated in a furnace, the film was heated homogeneously such that the whole film was converted to glass at the same time. On the other hand, due to the localized nature of the laser beam, sintering occurred in a small spot of the film while the rest of the area of the film remained at room temperature. Therefore, two stress models were set based on these two different heating situations. A fixed tensile strain was applied at one end of the substrate along the x direction to simulate the thermal stress induced by heating process of the coating, while the opposite end was fixed. For the laser sintering case, the strain was only applied to the substrate underneath the laser sintered area, but not to the rest of the film, since only the laser sintered region suffers shrinkage.

The stress distribution results of the FEM calculations are shown in Fig. 10. In the case of laser sintered, the induced stress was found to be about 9.1 MPa homogeneously in the sintered region. However, at the edge of the sintered region, the induced stress is dramatically decreased close to zero. On the other hand, in the case of furnace sintered films, a constant stress of about 9.2 MPa was found within the whole coating. Due to the large difference between the Young's modulus of the “hard” silica and the “soft” non-

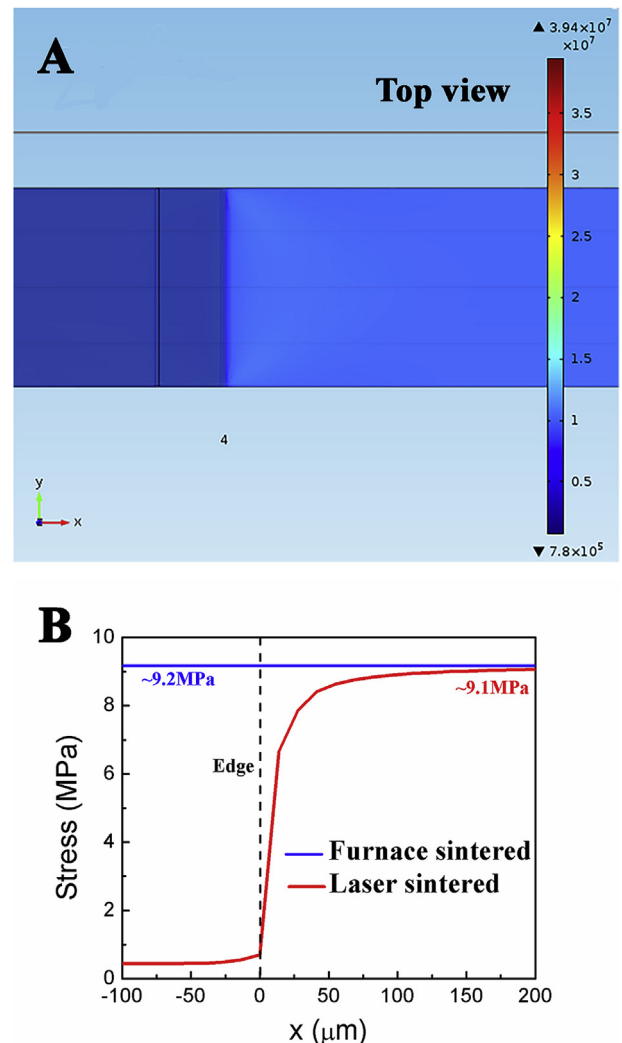


Fig. 10. (A) The calculated stress distribution of the top surface of the laser sintered film. (B) Stress distribution along the x direction at the interface between the laser sintered zone and the unsintered part.

sintered film, the thermally induced stress can be relaxed by the surrounding non-sintered film.

Cracking of the films induced by the heating process is related to the total volume of the heating zone. When the heating volume exceeds certain value, cracks will occur on the surface of the films. For a fixed film thickness, the area sintered by the laser beam can be

used to estimate the spacing between the cracks. If the dimension of the heating area is larger than the critical spacing of the cracks, cracking will occur. Since the dimension of the heating area cannot be controlled in furnace sintering, cracking will occur whenever the thickness of the film exceeds a certain value, the so-called critical thickness. On the other hand, laser sintering allows for precise control of the heating area. Consequently, as long as the laser sintered area is smaller than the predicted spacing between the cracks, cracking can be prevented even when the film exceeds the critical thickness. The spacing between the cracks was determined to be about 700 μm after furnace heating (Fig. 9A), which is similar to the width of the laser beam track thus effectively preventing cracking to occur during laser sintering (Fig. 9A).

4. Conclusion

Erbium-doped silica films were deposited by the dip-coating method from sol precursors and sintered by laser scanning and using a furnace. The shrinkage ratio of the sintered films was found to be about the same for both sintering methods. SEM imaging suggested the laser sintered film to have achieved a density similar to that of the fused silica substrate. Importantly, it was shown that laser scanning sintering is able to suppress cracks during sintering in relatively thick films (sintered thickness greater than 1 μm). A FEM model was developed to analyze the thermal stress distribution induced by sintering. The model showed that due to the localized sintering of the laser beam, sintering mismatch stresses are localized resulting in stressed volume being below the critical volume needed for cracking. Photoluminescence and radio-luminescence results on powders derived from doped gels confirmed that silica could be activated by rare earths to produce efficient luminescence.

Acknowledgement

This material is based upon work supported by the Department of Energy under grant DE-FE00012272, and the National Science Foundation under Grant No. 1207080.

Appendix A. Supplementary data

Supplementary data related to this article can be found at <http://dx.doi.org/10.1016/j.optmat.2017.03.035>.

References

- [1] L. Yang, S.S. Saavedra, Chemical sensing using sol-gel derived planar waveguides and indicator phases, *Anal. Chem.* 67 (1995) 1307–1314.
- [2] X. Orignac, D. Barbier, X. Min, R.M. Almeida, O. Mccarthy, E. Yeatman, Sol-gel silica/titania-on-silicon Er/Yb-doped waveguides for optical amplification at 1.5 μm , *Opt. Mater.* 12 (1999) 1–18.
- [3] A. García-Murillo, C. Le Luyer, C. Dujardin, T. Martin, C. Garapon, C. Pédrini, J. Mugnier, Elaboration and scintillation properties of Eu^{3+} -doped Gd_2O_3 and Lu_2O_3 sol-gel films, *Nucl. Instr. Meth. Phys. Res. A* 486 (2002) 181–185.
- [4] A. García-Murillo, C. Le Luyer, C. Dujardin, C. Pédrini, J. Mugnier, Rare-earth activated sol-gel films for scintillator applications, *J. Sol-Gel Sci. Technol.* 26 (2003) 1–4.
- [5] C. Ma, H. Li, H. Wu, Q. Fu, C. Sun, X. Shi, Y. Zhang, Z. Zhang, J. Tao, Z. Han, Mullite oxidation resistant coating for SiC-coated carbon/carbon composites by supersonic plasma spraying, *J. Mater. Sci. Technol.* 29 (2013) 29–33.
- [6] J. Hu, R.G. Gordon, Textured aluminum-doped zinc oxide thin films from atmospheric pressure chemical-vapor deposition, *J. Appl. Phys.* 71 (1992) 880–890.
- [7] C. Brinker, G. Scherer, *Sol-gel Science: The Physics and Chemistry of Sol-gel Processing*, Academic press, Inc., 1990.
- [8] M. Tong, G. Dai, D. Gao, WO_3 thin film sensor prepared by sol-gel technique and its low-temperature sensing properties to trimethylamine, *Mater. Chem. Phys.* 69 (2001) 176–179.
- [9] C. Mansuy, R. Mahiou, J.M. Nedelec, A new sol-gel route to Lu_2SiO_5 (LSO) scintillator: powders and thin films, *Chem. Mater.* 15 (2003) 3242–3244.
- [10] D.J. Taylor, B.D. Fabes, Laser processing of sol-gel coatings, *J. Non. Cryst. Solids* 147–148 (1992) 457–462.
- [11] B.D. Fabes, D.J. Taylor, L. Weisenbach, M.M. Stuppi, D.L. Klein, L.J. Raymond, B.J.J. Zelinski, D.P. Birnie III, Laser processing of channel waveguide structures in sol-gel coatings, *SPIE Sol-gel Opt.* 1328 (1990) 319–328.
- [12] M. Guglielmi, P. Colombo, L. Mancinelli Degli Esposti, G.C. Righini, S. Pelli, V. Rigato, Characterization of laser-densified sol-gel films for the fabrication of planar and strip optical waveguides, *J. Non-Cryst. Solids* 148 (1992) 641–645.
- [13] S. Pelli, G.C. Righini, A. Scaglione, M. Guglielmi, A. Martucci, Direct laser writing of ridge optical waveguides in silica-titania glass sol-gel films, *Opt. Mater.* 5 (1996) 119–126.
- [14] K.K. Lee, D.R. Lim, H.-C. Luan, A. Agarwal, J. Foresi, L.C. Kimerling, Effect of size and roughness on light transmission in a Si/SiO₂ waveguide: experiments and model, *Appl. Phys. Lett.* 77 (2000) 1617.
- [15] H. Unuma, Y. Suzuki, S. Sakka, Preparation of silica and glass fibers from tetraethylorthosilicate and hexamethyldisiloxane, *Nippon. Seramikkusu Kyokai Gakujutsu Ronbunshi* 97 (1989) 208–212.
- [16] C.A. Milea, C. Bogatu, A. Duta, The influence of parameters in silica sol-gel process, *Bull. Transilv. Univ. Brasov Eng. Sci.* 4 (2011) 59–66.
- [17] P.W. France in *Fluoride Glass Optical Fibers*, CRC Press, Boca Raton, FL, 1990, pp. 132–185.
- [18] M.S. Dhlamini, G.H. Mhlongo, K.T. Hillie, Effects of accelerating beam voltage on luminescence of Er^{3+} and Tm^{3+} doped SiO_2 phosphor prepared by sol-gel process, *Opt. Mater.* 33 (2010) 79.
- [19] J. Götze1, M. Plötze, D. Habermann, Origin, spectral characteristics and practical applications of the cathodoluminescence (CL) of quartz - a review, *Mineral. Petrol* 71 (2001) 225.
- [20] J.M. Sun, W. Skorupa, T. Dekorsy, M. Helm, A.N. Nazarov, On the mechanism of electroluminescence excitation in Er-doped SiO_2 containing silicon nanoclusters, *Opt. Mater.* 27 (2005) 1050.
- [21] Yu. Zorenko, V. Gorbenco, T. Zorenko, V. Savchyn, M. Batentschuk, A. Osvet, C. Brabec, Luminescent properties and energy transfer processes in YAG: Er single crystalline films, *J. Lumin* 154 (2014) 198.
- [22] J.C. Grosskreutz, M.B. McNeil, The fracture of surface coatings on a strained substrate, *J. Appl. Phys.* 40 (1969) 355–359.
- [23] M.S. Hu, M.D. Thouless, A.G. Evans, The Decohesion of thin films from brittle substrates, *Acta Metall.* 36 (1988) 1301–1307.

[1] L. Yang, S.S. Saavedra, Chemical sensing using sol-gel derived planar